Hindawi
Shock and Vibration
Volume 2023, Article ID 3631729, 14 pages
https://doi.org/10.1155/2023/3631729

Research Article

A Comparative Study on the Dynamic Tensile Strength Evaluation Method of Rock Materials

Se-Wook Oh,[1] Byung-Hee Choi,[1] Yong-Bok Jung,[1] and Sang-Ho Cho[2,3]

[1]*Deep Subsurface Storage and Disposal Research Center, Korea Institute of Geoscience and Mineral Resources, Daejeon 34132, Republic of Korea*
[2]*Department of Mineral Resources and Energy Engineering, College of Engineering, Jeonbuk National University, 4 Jeonju-si 54896, Republic of Korea*
[3]*Department of Energy Storage and Conversion Engineering, Graduate School, Jeonbuk National University, 9 Jeonju-si 54896, Republic of Korea*

Correspondence should be addressed to Sang-Ho Cho; chosh@jbnu.ac.kr

Received 14 December 2022; Revised 12 June 2023; Accepted 4 July 2023; Published 3 August 2023

Academic Editor: Carlo Rosso

The representative calculation methods of dynamic tensile strength applied to the spalling test are comparatively reviewed in the same experimental cases. The results are compared with those of the ISRM suggested dynamic BD method. Through comparative verification results and analysis of methodological characteristics of each determination method in the spalling test, the most reasonable method for calculating dynamic tensile strength in the high strain rate condition is derived. The local strain rate and apparent strain rate are calculated for the same experimental cases, and the difference in the result values according to the strain rate calculation technique is analyzed through comparative verification of the calculated results. Consequently, the characteristics of each dynamic tensile strength determination method and strain rate calculation method in the spalling test are presented, and the results of the review on the most suitable method for calculating the dynamic tensile strength of rock materials are presented.

1. Introduction

Rock materials consisting of bedrock and underground structures can easily be exposed to dynamic impact loadings such as rock blasting, percussion drilling, missile penetration, or earthquake. In order to predict the damages caused by those various impact loads, it is important to understand the fracture behavior of the rocks under dynamic loading conditions. Since many mining and civil engineering works are performed near one or more free surfaces, the rock mass can be severely influenced by tensile behavior. Furthermore, it is well known that rocks are much weaker in tension than in compression, and it generally shows rate dependency in the increment of the loading rate or strain rate, and the accurate determination of the dynamic tensile strength of the rock is crucial [1, 2]. However, due to the transient nature of loading and the complexity of dynamic phenomena, the dynamic tension test has many limitations and much more difficulties as compared to the static case.

According to the prior studies on the dynamic tension test for the rock materials, there were several experimental approaches, such as the Split Hopkinson Tension Bar (SHTB) test, Semicircular Bending (SCB) test, Brazilian Disc (BD) test, and the spalling test [3–5]. The dynamic tension test using the SHTB apparatus is a direct tension testing method that loads a specimen directly with tensile loading. It has the same principles as those applied to the static tests. However, as compared with the SHPB test, the techniques for gripping the rock specimen in the SHTB test are much more complicated [1]. Furthermore, the SHTB test forces to use the dog-bone-shaped specimen; this complicated specimen geometry makes the SHTB testing even more challenging. In order to improve those problems from the SHTB tests, several indirect tension testing methods have been extensively studied, such as the BD test, SCB test, and

the spalling test. Those indirect testing methods provide convenient alternatives for the experimental apparatus, data interpretation, and specimen manufacturing.

The BD test is most widely used to determine the dynamic tensile strength of rock materials due to its simple experimental procedures, such as the sample preparation and the calculation method. Several limitations of the BD test are also pointed out. For example, the specimen is subjected to a biaxial stress state and difficult to achieve the stress equilibrium state at high strain rate conditions because of the premature or local failure at the loaded area by the high compressive loading [6].

The SCB method uses a half-circular disc specimen to induce the bending fracture on the specimen by a three-point loading. According to the previous studies, it is reported to have a relatively lower strength value than the determining tensile strength by other testing methods because it is fractured by flexural tensile behavior [7, 8]. Finally, the spalling method uses the spall phenomenon based on the principle that compressive waves are reflected as tensile waves at solid materials' boundary. It is mainly applied to determine the dynamic tensile strength of brittle materials at high strain rates. The spalling method utilizes the stress wave reflection at the free surface, so a high level of loading/strain rate gives an advantage for conducting the tests. Furthermore, considering that the compressive strength of rock materials is known to be about 10 to 20 times higher than that of the tensile, the probability of damage caused by compression is extremely low in the experimental procedure, contrary to previous concerns. Accordingly, this study considered the dynamic tensile test for the rock materials at the high strain rate conditions using the spalling method and aims to improve the problems previously presented.

Numerous studies have been carried out in the last few decades concerning the spalling method [9–11]. Hino, one of the pioneers of dynamic tension tests on the blasting technique, developed a dynamic tensile fracture test with explosive shock loading based on spall phenomena [12]. Since that, several studies have been performed by many other researchers with the same experimental approach. For instance, Cho et al. performed a series of spalling tests with three types of rocks: Inada granite, Tage tuff, and Kimach sandstone [11]. From the application of numerical investigations, they reported that differences between static and dynamic tensile strengths are related to the stress concentration and redistribution mechanisms against the different loading conditions, mainly caused by the inhomogeneity of rock materials. Kubota et al. applied the spalling method to Kimach sandstone with various shock loadings controlled by different lengths of water-filled PMMA pipe [10]. They suggested an improved method to determine the dynamic tensile strength and strain rate by adopting the concept of averaged fractured points based on the free surface velocity measurement. There have been developed other loading technique for spalling test, which generates dynamic loading with the implementation of mechanical equipment such as the Split Hopkinson pressure bar (SHPB) [9, 13]. Kelpaczko and Brara investigate the dynamic tensile strength of microconcrete using the aluminum alloy Hopkinson bar apparatus [13]. They could calculate the transmitted stress wave onto concrete specimens from the Hopkinson bar with the strain gauge measurement and a theoretical assumption so that the wave analysis was used to determine dynamic tensile strength and strain rate in their study. Erzar and Forquin [9] measured the free surface velocity of the concrete specimen with a laser vibration sensor and accelerometer to estimate the dynamic tensile strength, and attached strain gauges calculated the strain rate on the specimen nearby spall failure.

Confusions arise regarding the specific method to determine dynamic tensile strength. Even if all the spalling tests were conducted with the same principles, there are many differences in determining the dynamic tensile strength. It is also complicated to compare the results or methodologies of previous studies to a proper degree because of the differences in rock types, size, and experimental conditions. Consequently, objective and standardized comparison between current methods is strongly required.

The purpose of this study is to practically study respective methods for determining the dynamic tensile strength of rock materials and its standardized comparison (so that we can estimate the dynamic tensile strength more accurately). Three conventional determination methods in the spalling test were simultaneously applied to each experiment in this paper. In order to minimize the influence of nonmechanical factors (i.e., temperature, specimen size, and rock type), the experimental conditions were strictly controlled to be the same in each experiment. The Hopkinson pressure bar system was used to load rock specimens dynamically because it has many advantages in stress wave control, measurement, and repeatable operation. A series of static and dynamic Brazilian Disc (BD) tests were conducted and compared to this study's determined dynamic tensile strength. Furthermore, from the measurement of local strain and strain rate near the spall fracture on rock specimens, the influence of the determined strain rate by different methods was also discussed in this study.

2. Experimental Methods

2.1. Determination Method for Dynamic Tensile Strength in the Spalling Test. Current methodologies for empirically determining dynamic tensile strength via spalling tests can be bifurcated into two principal categories: the method predicated on spalling block velocity and the method founded on pullback velocity. Furthermore, the spalling block velocity method is subdivided into two distinct approaches: one that computes strength predicated on the incident stress wave within the specimen and another that estimates strength based on the particle velocity at the specimen's free surface terminus. This paper has defined the determination methods into three categories to prevent confusion. The spalling block velocity method is categorized into SBV-1 and SBV-2, while the pullback velocity method is denoted as PV. Detailed information about each method is provided in the following sentences.

The SBV-1 method has been employed by several researchers operating within the domains of rock dynamics and blasting engineering to determine the dynamic tensile

strength under high strain rate conditions of rock materials [10–12]. Historically, dynamic loading resulting from detonation was primarily facilitated by affixing a detonator or explosive, accompanied by a metal plate and a water pipe, to one side of a cylindrical rock specimen. However, due to the inherent challenges associated with recurrent experiments and the constraints imposed by the usage of explosives, recent investigations have shifted towards the utilization of dedicated experimental apparatuses, such as Hopkinson bars. Figure 1 illustrates the basic configuration of the SBV-1 scheme. A dynamic load is administered at one extremity of the specimen, while the particle velocity is gauged at the opposing end using a laser displacement sensor or a vibration meter. Furthermore, high-speed camera imaging is conducted from the side, facilitating the inspection of the initial fracture location within the specimen.

The stress σ at the arbitrary point proximate to the free plane of the specimen can be determined as follows [10]:

$$\sigma = \frac{\rho_1 C_1}{2} \{-v(t) + v(t - 2\Delta t)\}, \tag{1}$$

$$\Delta t = \frac{x}{C_1}, \tag{2}$$

where ρ_1, C_1, and $v(t)$ are the density, the longitudinal wave velocity of the rock specimen, and the particle velocity at the free surface. x is the distance from the free surface at the arbitrary point. The first term encapsulated in curly brackets represents the compression wave, while the second corresponds to the tensile wave. This construct is available from $t > 2\Delta t$ [10–12]. Two underlying assumptions are inherent to this formulation: firstly, the phenomenon is considered to be one-dimensional, and secondly, the stress wave remains stable proximate to the free surface. To estimate the dynamic tensile strength, the arbitrary point is designated at the fracture surface, introducing an additional assumption that fracture occurs when the peak of the stress wave associated with the tensile component reaches the fracture surface. From the substitution of $t_p + 2\Delta t$ for t in equation (1), the dynamic tensile strength σ_t can be determined at a fractured position as follows [10]:

$$\sigma_d = \frac{\rho_1 C_1}{2} \left\{-v\left(t_p + 2\Delta t\right) + v\left(t_p\right)\right\}, \tag{3}$$

$$\Delta t = \frac{x_f}{C_1}, \tag{4}$$

where t_p is the rise time of stress history to the peak stress and x_f is the distance from the free surface to the fractured position. x_f can be measured by recovering the fractured specimen for the single failure. If multiple failures have occurred, the first fracture plane should be investigated using high-speed camera observation.

The SBV-2 method has been used to determine the dynamic tensile strength of rocks and concretes, and it aligns with the theoretical underpinnings of the SBV-1 approach. However, distinctions are observed in the data types used to calculate dynamic tensile strength and the corresponding data acquisition methods. The most significant point of divergence between the two methodologies is that SBV-1 employs free surface particle velocity to calculate stress at a specific point within the specimen, whereas SBV-2 utilizes the stress wave profile incident on the specimen. Consequently, the SBV-2 approach necessitates specific apparatus to measure information on incident stress waves, such as the Hopkinson pressure bar. At the same time, there is no requirement for any instrumentation to gauge the particle velocity of the free surface. Figure 2 presents the experimental design of the SBV-1 method. As illustrated in Figure 2, a metallic bar and a cylindrical rock sample are arranged along a common axis, with one extremity of the bar and the specimen making contact. A dynamic load is applied to the opposite end of the bar surface, enabling the measurement of the stress wave profile propagating along the metallic bar via a strain gauge affixed to the rod's surface. When the incident stress wave reaches the bar-specimen interface, a portion of the wave is transmitted into the specimen, and the remains are reflected back to the metal bar as a tensile wave. In an ideal scenario where the bar-specific interface adheres to an ideal state, calculations can be straightforwardly performed utilizing one-dimensional wave propagation theory [14]. Nevertheless, given the difficulty in satisfying this ideal condition during empirical investigations, a more direct approach widely used in rock dynamic experiments using SHPB systems to ensure reliability was also adopted [1, 2]. This involved calculating the wave history transmitted to the test specimen by superimposing the incident wave and the reflected wave, which were traced synchronously through waveform progression over an identical time span (see Figure 3).

The estimation of dynamic tensile strength A using the SBV-2 method according to equations (3) and (4) mentioned above is as follows:

$$\sigma_d = -\sigma\left(t_p + 2\Delta t\right) + \sigma\left(t_p\right). \tag{5}$$

The PV method, initially introduced by Novikov [15], has since been further advanced and refined by a series of subsequent researchers [9, 16]. This method entails inferring stress behavior within a specimen and determining the dynamic tensile strength through the interpretation of the time-particle velocity curve measured on the free surface of the specimen. A general experimental setup is shown in Figure 4. Measurement of incident stress waves on a specimen or observation of a fracture position using a high-speed camera is not mandatory. However, the strain gauge is required to be attached to the specimen to measure the strain rate.

Figure 5 shows a typical free surface particle velocity profile in the spalling test against time. At point A in time, the compressive stress wave arrives at the free surface of the specimen, after which the particle velocity swiftly escalates to its apex to time B. The free surface particle velocity then gradually decreases to point C, where the difference between the velocity at point B and at point C is called pull-back velocity. At point C, a fracture plane is

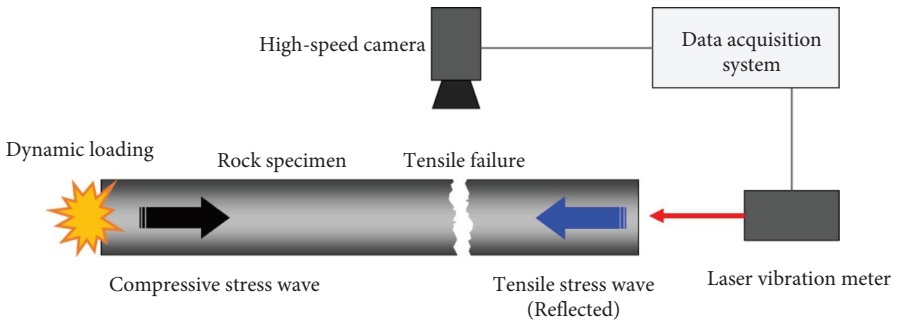

Figure 1: Schematics of the spalling test using SBV-1 method.

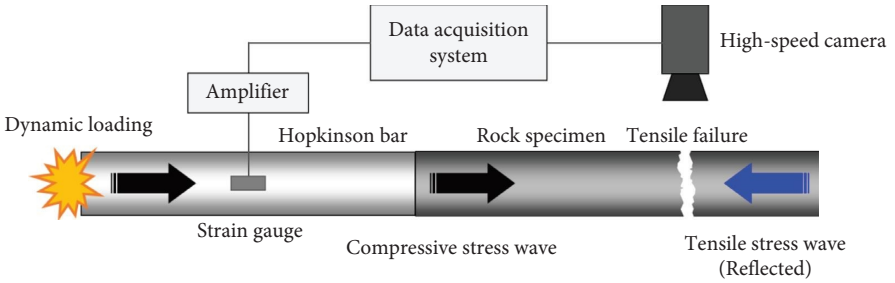

Figure 2: Experimental configuration of the SBV-2 method in the spalling test.

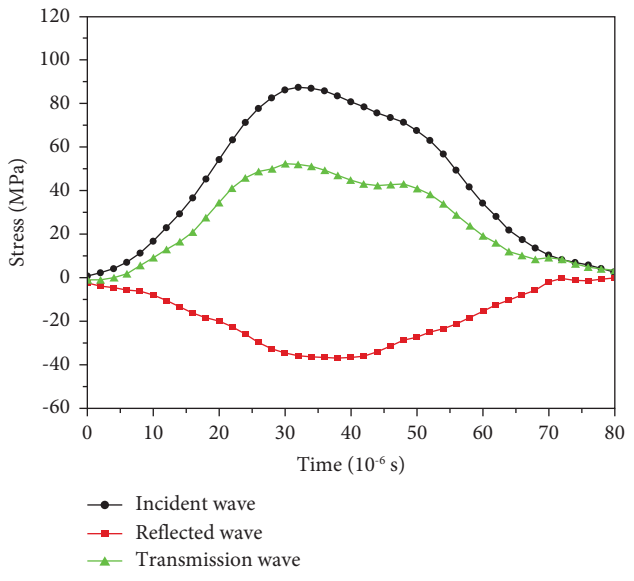

Figure 3: Determination of transmitted stress wave into rock specimen at the bar-specimen interface by stress wave superimposition (wave profile was used from Exp. ID: SP-02).

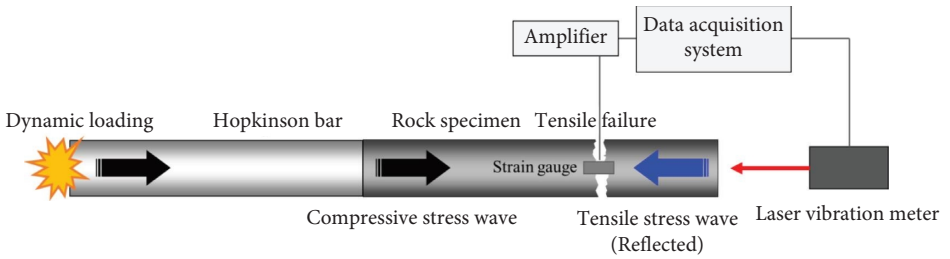

Figure 4: Experimental configuration of the PV method in the spalling test.

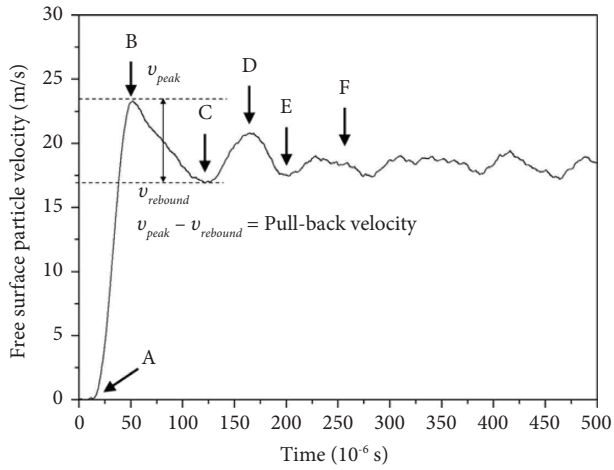

FIGURE 5: Interpretation of the free surface particle velocity profile in the PV method (FSPV curve was used from Exp. ID: SP-02).

formed by tensile stress, and the particle velocity increases again to point D due to the separation of the specimen. At point D, under the influence of a newly emerging tensile stress wave, particle velocity diminishes until point E. Subsequent behavior, including point F, exhibits a scattering motion at a consistent rate, accompanied by intermittent oscillations. Consequently, based on the wave propagation process and the fracturing behavior, the dynamic tensile strength can be deduced by the free surface particle velocity as follows [15]:

$$\begin{aligned}\sigma_d &= \frac{\rho_1 C_1}{2}\, v_{\text{peak}} - v_{\text{rebound}} \\ &= \frac{\rho_1 C_1}{2}\, v_{\text{pull-back}}.\end{aligned} \tag{6}$$

2.2. Determination of the Strain Rate in the Spalling Test. Since the dynamic properties of the rock materials exhibit loading/strain rate dependency, they require to be presented with corresponding loading/strain rate for each mechanical property (e.g., strength). In the spalling test, obtaining direct measurements of the deformation behavior of the specimen's failure region proves challenging. Consequently, the strain rate is indirectly deduced by leveraging the stress wave or the FSPV profile, or it can be locally measured via a strain gauge positioned at the fracture.

Three estimation methods exist for the strain rate: apparent strain rate, modified apparent strain rate, and local strain rate. The apparent strain rate $\dot{\varepsilon}_{\text{app}}$ can be calculated by applying the deformation to the entire length of the specimen, as shown in equation (7). The modified apparent strain rate $\dot{\varepsilon}_{m-\text{app}}$ has been proposed to compensate for the problems of the conventional apparent strain rate calculation. It uses the length of the fragments instead of the whole specimen length, as shown in equation (8) [10]. Finally, the local strain rate $\dot{\varepsilon}_{\text{local}}$ uses the obtained direct strain data from the strain gauge attached to the expected failure area of the specimen [10, 11].

$$\begin{aligned}\varepsilon_{\text{app}} &= \frac{\int_0^{t_p} 0.5\, v(t)\mathrm{d}t}{L}, \\ \dot{\varepsilon}_{\text{app}} &= \frac{\varepsilon_{\text{app}}}{t_p},\end{aligned} \tag{7}$$

$$\begin{aligned}\varepsilon_{m-\text{app}} &= \frac{\int_0^{t_p} 0.5\, v(t)\mathrm{d}t}{L_f}, \\ \dot{\varepsilon}_{m-\text{app}} &= \frac{\varepsilon_{\text{app}}}{t_p},\end{aligned} \tag{8}$$

where ε_{app} and $\varepsilon_{m-\text{app}}$ indicate the apparent strain rate and modified apparent strain, respectively. L is the length of the specimen, and L_f is the length of fragments.

2.3. Dynamic Brazilian Disc Test. The BD test is the most popular method for determining the tensile strength of the rock materials for both dynamic and static loading conditions [17]. It uses the disc-type specimen and loads the side part with the same axis to induce tensile failure at the center of the specimen. Figure 6 shows the general experimental setup for the dynamic BD test [5].

The dynamic BD method shares the calculation theory for the tensile strength with the static method; therefore, the stress equilibrium state within the specimen should be achieved. Finally, the dynamic tensile strength in the BD test σ_{dt} can be determined by equation (9) as follows [5]:

$$\begin{aligned}\sigma_{dt} &= \frac{2P_t}{\pi DT}, \\ P_t &= \pi r^2 \sigma_{t\,\max},\end{aligned} \tag{9}$$

where P_t is the maximum force, and D and T are the diameter and thickness (height) of the specimen, respectively. r is the diameter of the bars, and $\sigma_{t\,\max}$ is the maximum stress of the transmitted wave.

Similar to the spalling test, the strain rate calculation in the Dynamic Brazilian Disc test encompasses indirect and direct calculation methodologies. The indirect approach assumes linear behavior, and apparent strain rate $\dot{\varepsilon}_{\text{app}}$ can be executed via equation (10) [5]. The direct method entails measuring the strain rate by affixing a strain gauge to the central surface of the specimen, where tensile failure occurs [5].

$$\begin{aligned}\varepsilon_{\text{app}} &= \frac{\sigma_{dt}}{E}, \\ \dot{\varepsilon}_{\text{app}} &= \frac{\varepsilon_{\text{app}}}{t_p}.\end{aligned} \tag{10}$$

3. Experiments

3.1. Experimental Setup and Procedures. A series of dynamic tension tests using the Hopkinson pressure bar system was conducted to determine the dynamic tensile strength of the Hwangdeung granite. The conventional SHPB system was

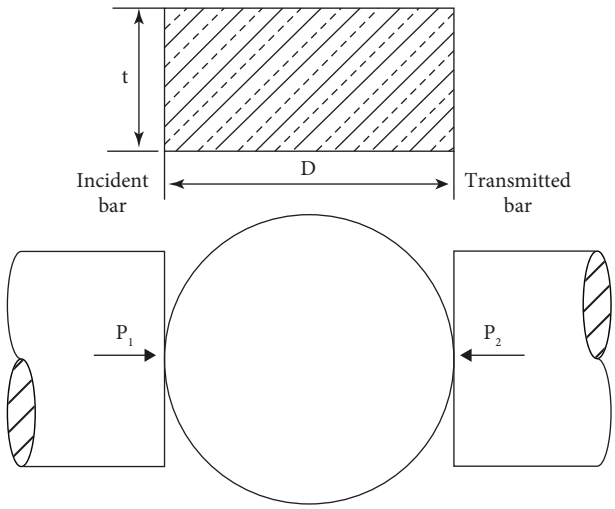

Figure 6: Schematics of the dynamic BD test using SHPB apparatus [5].

applied to the dynamic BD test, as shown in Figure 7(a). The Split Hopkinson Pressure Bar (SHPB) system, predicated on the alignment of three metal rods on the same axis, is recognized as an ideal apparatus for conducting material property experiments ranging from 10/s to 10^4/s strain rates [1]. The rock specimen is positioned between two metal bars, the incident and transmission bars. A striker bar, propelled by the launching system, impacts one side of the incident bar, dynamically loading the specimen. Information regarding the stress waves within the system can be procured through a pair of strain gauges affixed to the surfaces of the incident and transmission bars, respectively.

Leveraging the principles of one-dimensional wave theory, the dynamic forces exerted on the end face of both the incident bar P_1 and the transmission bar P_2 in contact with the specimen can be computed as follows [1]:

$$\begin{aligned} P_1 &= AE(\varepsilon_i + \varepsilon_r), \\ P_2 &= AE\varepsilon_t, \end{aligned} \tag{11}$$

where A is the cross-sectional area and E is Young's modulus of the bars. ε_i, ε_r, and ε_t are the incident, reflected, and the transmitted strain signal, respectively. In this study, a dynamic Brazilian Disc test was conducted utilizing the SHPB system made of 38 mm diameter maraging steel. The incident bar and transmission bar lengths are 2,200 mm and 1,800 mm, respectively. The bars exhibit a longitudinal wave velocity of 5,474 m/s and Young's modulus of 246 GPa. In order to observe the fracture behavior, high-speed camera imaging was employed, and information on stress waves obtained through strain gauges was recorded and analyzed via digital oscilloscopes. For the dynamic BD test, the pulse shaping techniques using a copper disc pulse shaper were applied to achieve the stress equilibrium state within the specimen.

Figure 7(b) presents the single Hopkinson pressure bar system for the spalling test. The basic characteristics of the system are the same as that of the SHPB system, and there is a difference in removing the transmission bar to maintain one end surface of the test piece as a free plane. A laser displacement sensor with a resolution of 392 kHz was additionally applied to measure the specimen's free surface particle velocity of the specimen, and the strain gauges were attached to the free surface of each test piece to calculate the local strain rate. Image observation using a high-speed camera was also applied, like the BD experiment, to calculate the destructive behavior of the test piece and the initial fracture surface, and the photographing resolution was performed at 80,000~100,000 fps.

3.2. Specimen Preparation. Cylindrical and disc-shaped Hwangdeung granite specimens were manufactured for the spalling and the dynamic BD test. Since it is well known that granitic rocks exhibit strong anisotropy induced by the internal microcracks orientation, the specimens were designed to induce the tensile fracture in the same orthogonal plane direction by investigating the P-wave velocity of the block [18–20]. Table 1 shows the measured P-wave velocity for three orthogonal directions of the block. The P-wave velocity of the X and Y directions shows similar values, while that of the Z direction has a much lower value. Thus, the specimens were manufactured to have the Z plane as an expected failure plane, as shown in Figure 8. All of the specimens were collected through coring in the same rock block, and the cross section was precisely processed to show an error within 0.01 mm. In consideration of the characteristics of natural materials showing unevenness and anisotropy, intact rock was used as a sample, and the inspection method using CT scan is also worth considering in the future to increase the quality of the specimen. The experiment used eight 250 mm spalling specimens, four 150 mm long specimens, and 15 dynamic BD specimens with a diameter of 50 mm and a length of 25 mm. The average physical and mechanical properties of the specimens are listed in Table 2.

4. Results and Discussion

4.1. Experimental Results. This research aims to apply various methods and conditions used in existing spalling tests on different rock materials to the same specimen and experimental conditions and to comparatively analyze the main characteristics and results of each strength and strain rate calculation method. The main experiment was a spalling test conducted on specimens with a diameter of 38 mm and a length of 250 mm. In order to examine the influence of the apparent strain rate due to changes in specimen length, additional tests were conducted using specimens of 150 mm length. A comparative indirect trend analysis was also carried out through the most commonly used dynamic BD test to determine the dynamic tensile strength of rock materials. The experimental results of the spalling and the

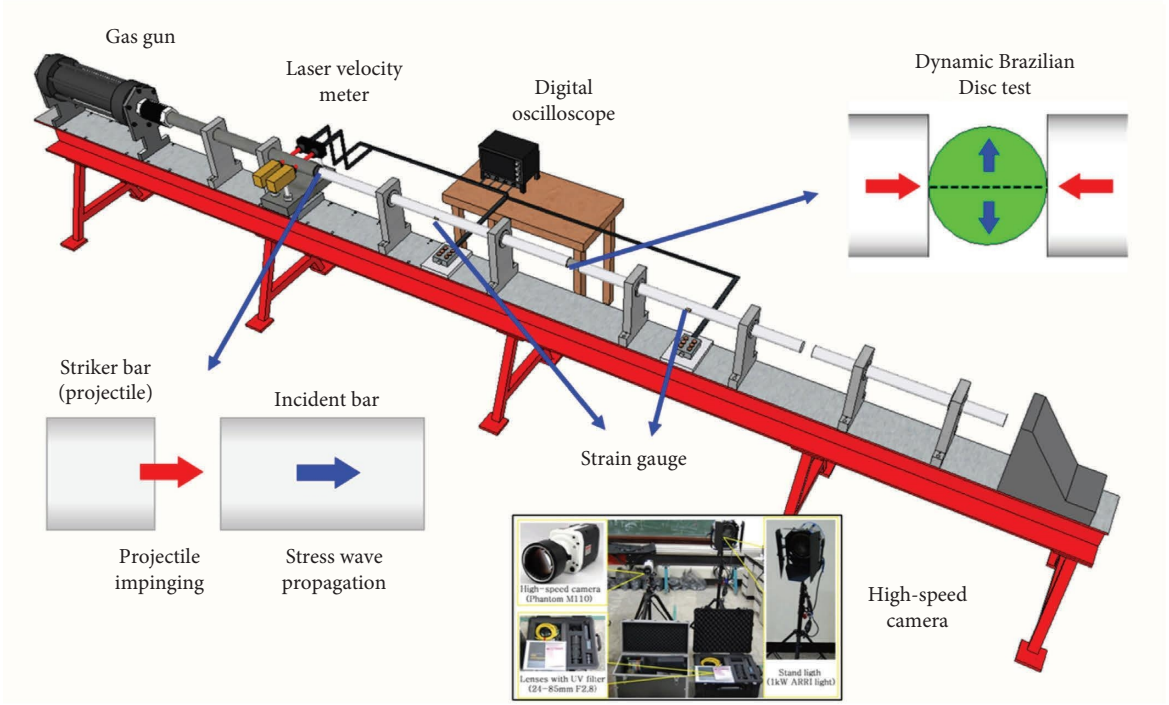

Figure 7: Schematics of experimental setup for determining the dynamic tensile strength of rock: (a) conventional SHPB system setup for the dynamic BD test and (b) single Hopkinson pressure bar system setup for the spalling test.

dynamic BD tests are described in Tables 3 and 4, and the calculated strain rate and dynamic tensile strength are indicated for each experimental case.

Figure 9 is a photograph of the fractured specimens after the experiment. In the case of multiple fracture surfaces, the first fracture surface determined by the high-speed camera is marked.

Table 1: Measured P-wave velocity of rock block with three orthogonal directions.

Direction	X	Y	Z
P-wave velocity (m/s)	4,151	4,069	3,515

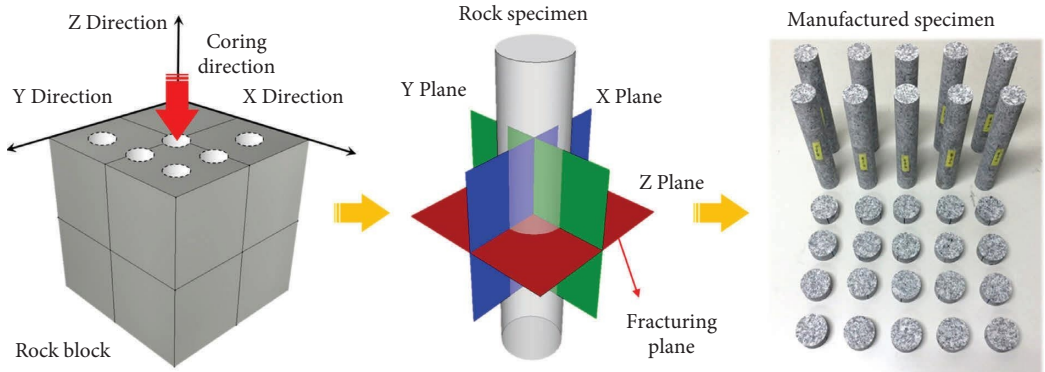

Figure 8: Specimen preparation procedure.

Table 2: Basic properties of the specimen.

Parameter	Value
Diameter (mm)	38, 50
Height (mm)	150, 250, 25
Density (kg/m^3)	2,617
Static compressive strength (MPa)	133
Static tensile strength (MPa)	5.7
Young's modulus (GPa)	31.41
Poisson's ratio	0.21

In all experimental cases, no macroscopic fracture was observed near the bar-specimen interface, and since the tensile deformation was about 5 to 20 times weaker than compression in rock materials, it was assumed that there was no damage due to compression near the pressurized surface.

4.2. Validation of the Stress Equilibrium State for the Dynamic BD Test. As with general SHPB tests, the dynamic BD tests require the achievement of the stress equilibrium state within the specimen as well as the validation for the proper tensile fracture in the central point. Figure 10 shows the plot of the stress equilibrium curve from one of the experimental results. It can be found that the green-lined superimposed wave between the incident and reflected wave appears in good agreement with the transmitted wave, which draws as the blue line.

The snapshot of the high-speed camera images for the dynamic BD test is depicted in Figure 11. In the figure, the crack appears initiated from the center of the specimen at 60 μs; then, it propagates to the horizontal directions. In 180 μs, the local fracture is observed at the side of the specimen; however, it occurs after the central tensile crack is sufficiently extended, so it does not affect the test results.

4.3. Difference of the Estimated Dynamic Tensile Strength according to the Determination Methods. Three different calculations from the methods SBV-1, SBV-2, and PV, mainly used to determine the dynamic tensile strength for the spalling tests, were applied to the same experimental cases and compared to the results of the dynamic BD tests. Figure 12 illustrates the dynamic tensile strength of Hwangdeung granite deduced by each method for the strain rate.

The estimated dynamic tensile strength values were different according to the calculation method, even if they were from the same experimental case. The strength values calculated by the SBV-1 and the PV have similar results, but the calculated results of SBV-2 exhibit significantly higher values than others. The dynamic tensile strength determined by the BD test tends to be most similar to that of the PV. This can be assumed to be the difference in the data measurement methods underlying the strength calculation of the SBV-2. Unlike other methods, the SBV-2 theoretically reconstructs the stress distribution at the time of fracture based on the stress wave histories measured at the incident bar rather than the rock specimen. According to the previous studies, contrary to the static case, the dynamic fracture process of the rock materials is known to produce multiple small cracks with instantaneous high fracture energy. Through their growth and connection, the final fractures occur [5, 10]. For example, Cho et al. [11] investigated the fracture mechanism of the spalling test under different strain rate conditions using FEM analysis [5]. Their results showed that at the low strain rate corresponding to the static (or quasi-static) state, relatively large cracks were generated along the vulnerable parts in the specimen to form a failure plane.

On the other hand, under the high strain rate condition as a dynamic state, numerous microcracks occurred in the stress concentration area, and the failure plane was confirmed through their growth and connections. From the same perspective, it is deduced that the SBV-2, which

Table 3: Experimental results of the spalling test.

ID	Specimen length (mm)	Strain rate (1/s)			Dynamic tensile strength (MPa)		
		$\dot{\varepsilon}_{app}$	$\dot{\varepsilon}_{m-app}$	$\dot{\varepsilon}_{local}$	$\sigma_{dt,SBV-2}$	$\sigma_{dt,SBV-1}$	$\sigma_{dt,PV}$
SP-01	250	9.24	26.86	45.67	49.68	9.89	12.42
SP-02	250	11.91	32.04	41.30	50.15	10.38	12.10
SP-03	250	13.53	29.93	84.05	63.28	13.97	14.28
SP-04	250	17.14	48.72	113.99	59.85	14.06	20.49
SP-05	250	18.88	67.46	108.77	71.80	17.78	23.35
SP-06	250	19.68	56.57	104.24	75.61	10.88	23.49
SP-07	250	22.49	69.11	145.55	76.72	22.99	26.07
SP-08	250	23.49	72.05	140.81	74.83	16.64	24.58
SP-09	150	13.48	—	36.38	—	—	10.35
SP-10	150	42.59	—	124.12	—	—	26.01
SP-11	150	16.94	—	87.98	—	—	17.32
SP-12	150	32.68	—	97.65	—	—	19.47

Table 4: Experimental results of the dynamic BD test.

ID	Specimen (mm)	Strain rate (1/s)		Dynamic tensile strength (MPa)
		$\dot{\varepsilon}_{app}$	$\dot{\varepsilon}_{local}$	$\sigma_{dt,BD}$
BD-01	D50, L25	4.79	24.29	8.95
BD-02		4.01	23.18	8.75
BD-03		3.90	26.04	8.40
BD-04		2.86	18.46	7.57
BD-05		7.91	55.64	13.41
BD-06		5.95	43.96	11.96
BD-07		6.71	31.93	10.79
BD-08		11.73		14.75
BD-09		14.10		17.73
BD-10		15.44		18.96
BD-11		5.58		8.36
BD-12		10.43		12.30
BD-13		9.83		12.95
BD-14		15.70	—	19.74
BD-15		17.70		20.14

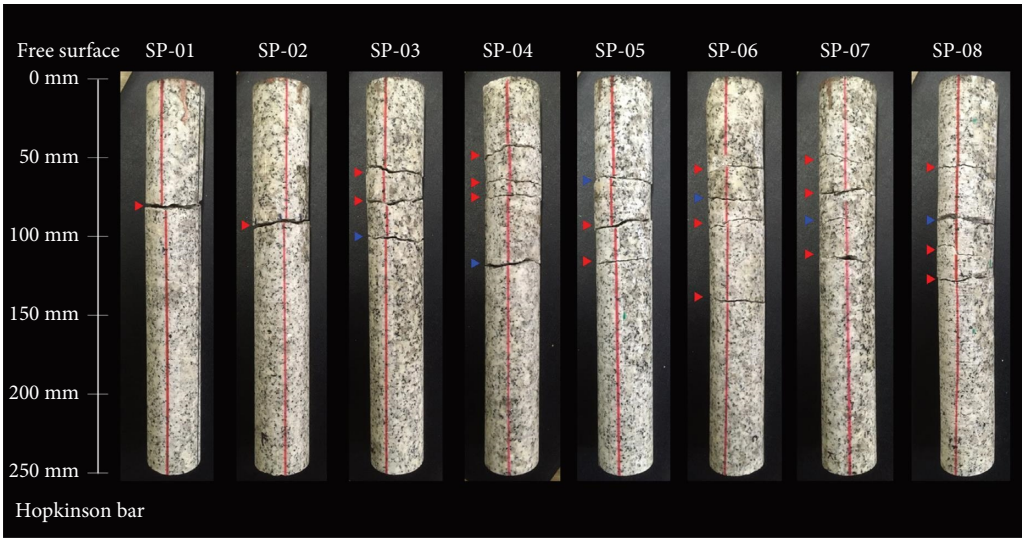

▶ = Fracture position

▶ = First fracture position captured by HSC

Figure 9: Photographs of fractured 250 mm length specimen after the spalling test.

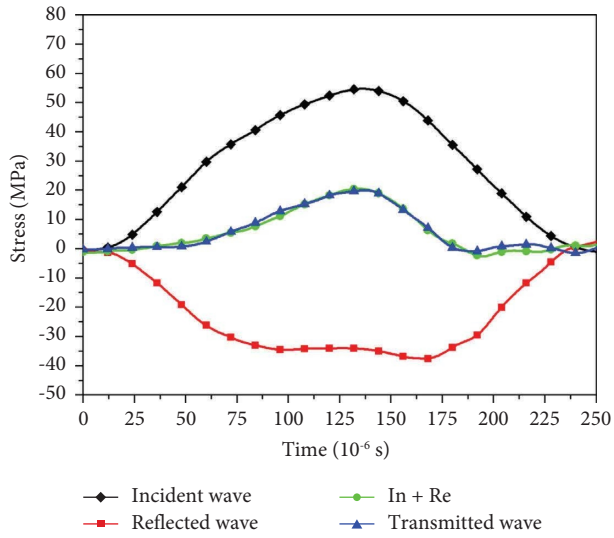

Figure 10: Stress equilibrium curve from the dynamic BD test result (Exp. ID: BD-15).

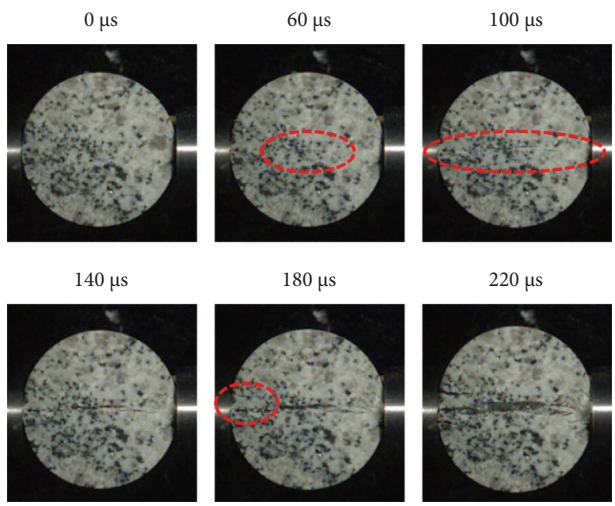

Figure 11: Verification of the fracture behavior on the specimen with high-speed camera observation (Exp. ID: BD-15).

uses indirect behavioral information of the specimen, cannot reflect the stress release and the fracture energy loss in the dynamic fracture process of the rock specimen. This results in a higher stress value than that is required for the actual failure of the rock specimen; consequently, the dynamic tensile strength is assumed to have been overestimated.

Another notable point in the abovementioned experimental results is the difference between the values of dynamic tensile strength calculated by the SBV-1 and the PV. The strength values calculated by the two methods show a similar tendency. However, the SBV-1's values appear relatively lower than those of the PV and exhibit high dispersion. In addition, the values calculated by the PV are more like the results of the dynamic BD tests.

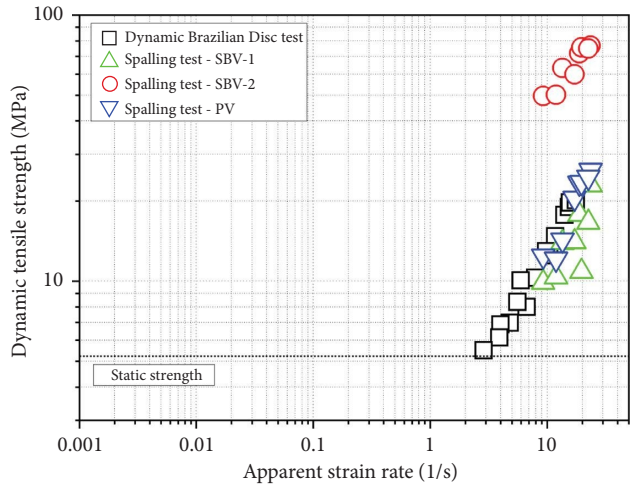

Figure 12: Comparison of the dynamic tensile strength estimated from different methods corresponds to the apparent strain rate.

The methodological difference between the two methods is based on the evaluation method for the specimen's failure position. For the SBV-1, the strength is estimated using the location of the first fracture captured by the high-speed camera. Meanwhile, the PV determines the strength of the fracture plane's location based on the interpretation of the FSPV curve, indicating the behavior of the specimen. As discussed earlier, it is closely related to the dynamic fracture process of the specimen. It can be seen as a matter of where to estimate the location that caused the specimen to be a significant failure.

As the previous studies claim, during the dynamic fracture process of the specimen, numerous cracks occur in the stress-intensive area, and the significant failure of the specimen occurs in this damage zone. The detection of the first fracture plane by the high-speed camera image is a macroscopic estimation that does not consider the internal fracture behavior of the specimen. As shown in Figure 13, in the high-speed camera images, the subsequent fracture can be observed on the separated pieces from the specimen body after the first failure. It can be evident as the basis for the preceding arguments.

Therefore, based on the high-speed camera images, the position of the resultant failure plane is transformed into a function of time on the FSPV curve as depicted in Figure 14. In Figure 14, capital A is the point at which the first fracture was captured through the high-speed camera image. In contrast, the time of failure estimated by the PV based on the failure behavior of the specimen corresponds to point C on the FSPV curve. As a result of reassigning the failure position of the specimen applied to the SBV-1 method, the dynamic tensile strength value was newly evaluated, as shown in Figure 15.

In Figure 15, the SBV-1 with modified first fracture position results showed a significant difference from the previous values and appeared similar to the PV and dynamic BD. The similarity between SBV-1 and PV results means that the determination of the failure position through the PV is well matched with the actual specimen failure.

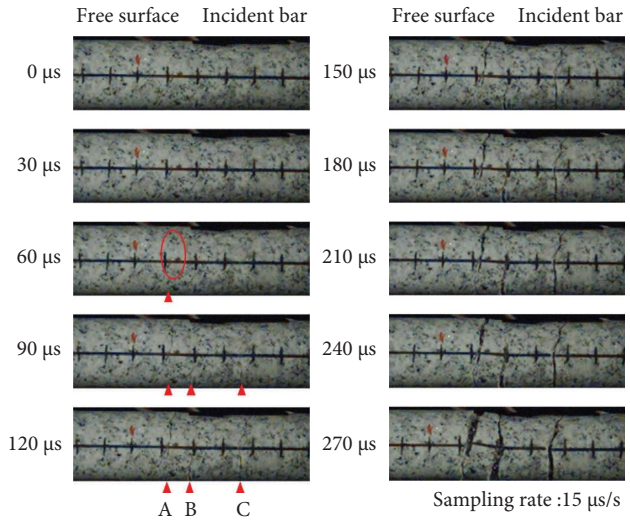

Figure 13: Determination of the first fracture position by high-speed camera observation (Exp. ID: SP-10, frame resolution: 70,000 fps).

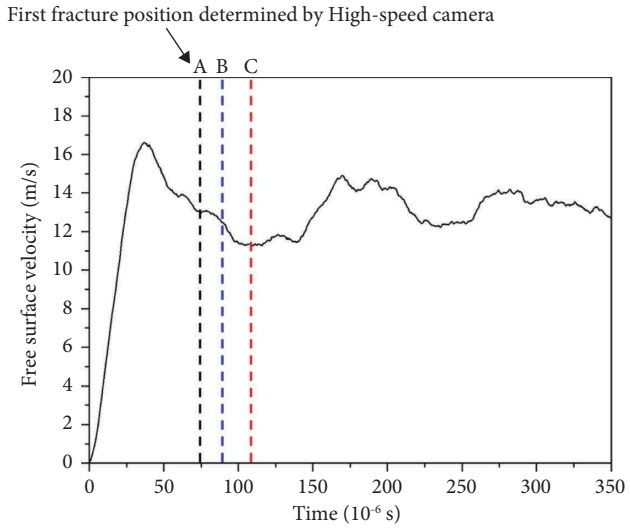

Figure 14: Detected fracture positions on the FSPV curve.

Consequently, methods of determining the failure location by macroscopic observations, such as high-speed camera imaging, cannot clearly reflect the dynamic fracture process of the specimen and suggest that it may act as an error factor in calculating the dynamic tensile strength.

4.4. Comparison of the Apparent Strain Rate with the Local Strain Rate. Since the dynamic properties of rock materials exhibit significant loading/strain rate dependency, it requires to be indicated together with the corresponding loading/strain rate [1, 2, 21, 22]. However, in the case of dynamic tensile testing, like the strength evaluation method, several different methods are used together to calculate the strain rate, and it still has been argued [5, 9, 10, 13]. Typical methods for calculating strain rate in dynamic tensile tests include calculating the apparent strain rate and the local

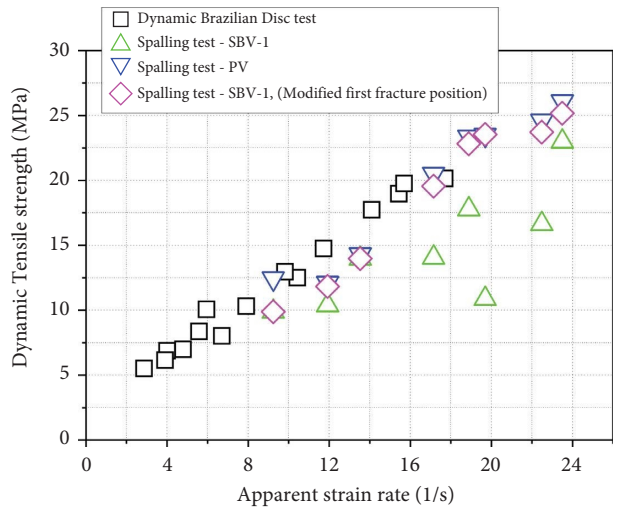

Figure 15: Comparison of the dynamic tensile strength determined by the SBV-1, PV, and the SBV-1 with modified first fracture position.

strain rate [5]. The apparent strain rate is calculated by converting the stress value acting on the specimen to the strain rate based on the theoretical analysis. However, it is not calculated solely for the points of failure in the specimen; thus, it is likely to be rated lower than the strain rate applied to the actual test specimen. The local strain rate is determined by attaching a strain gauge to the expected failure point of the specimen and calculating the value recorded by the gauge directly. Since the local strain rate method accepts the recorded value through the gauge as the strain data, it is pointed out that the result value is overvalued [9, 13]. Therefore, this study calculated the local strain rate by attaching strain gauges to the expected failure points of dynamic BD and the spalling specimen. The results were compared with the apparent strain rate speed values. Note that this section applied Method C to determine the dynamic tensile strength in the spalling test.

Figure 16 illustrates the determined, dynamic tensile strength values in the BD and spalling tests corresponding to the apparent and local strain rates. When the same strain rate calculation method was applied, the result values of the BD and spalling tests tended to be well matched, but there was a significant difference between the apparent strain rate and the local strain rate. In the case of the spalling test, the apparent strain rate value has a problem that depends on the length of the specimen. To compensate for these problems, Kubota et al. proposed a method of calculating the modified apparent strain rate using only the length of a piece of a separate test piece, such as (8) [10]. Thus, to identify the problems in calculating strain rate, as mentioned above, spalling tests were performed using different specimen lengths. The determined, dynamic tensile strength values were compared in Figure 17.

Figure 17 shows that the apparent strain rate value of the 150 mm specimen represents a value greater than that of the 250 mm specimen. In the case of modified apparent strain that considers only the length of the fragmented part of the specimen, the values of the local strain rate and the apparent

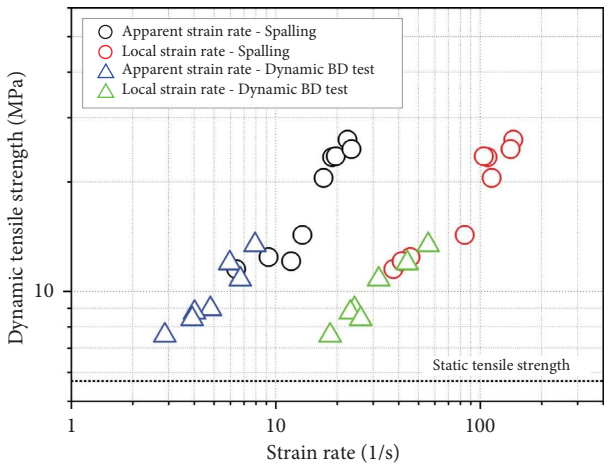

Figure 16: Dynamic tensile strength plotted with different strain rates.

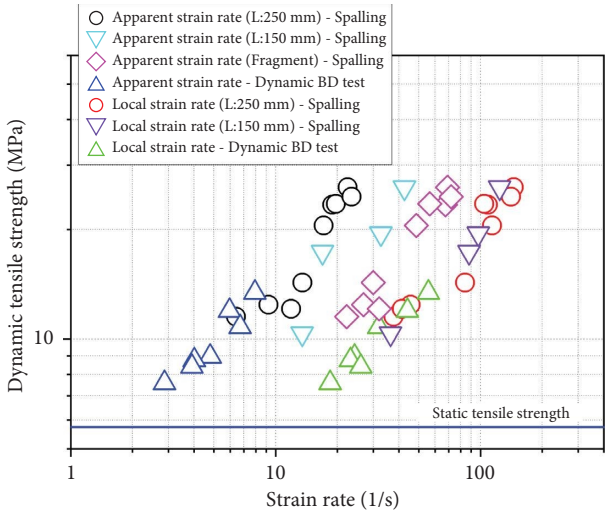

Figure 17: Dynamic tensile strength plotted with different strain rates by applying the various specimen lengths.

strain rate have appeared in the middle. These results indicate the limitations of the apparent strain rate calculation method, which applies the total size of the test specimen to the strain rate calculation, not limited to the fractured portion.

Although there is a clear difference in values depending on the method of calculating the strain rate, it was confirmed that the increased tendency of the dynamic tensile strength due to the increase in the strain rate was almost similar. This can be deduced to the apparent strain rate reflecting the deformation and fracturing behavior quite well, even if there is uncertainty in terms of scale.

The dynamic increase factor (DIF), defined as the ratio of dynamic strength to static strength, was calculated and compared with previous research results to analyze the meaning of the difference in results according to the strain rate calculation method. Figure 18compares the dynamic tensile strength reported from the previous studies and the results of this study employing a DIF curve [10, 11, 23–29]. As a result, the dynamic tensile strength values expressed at

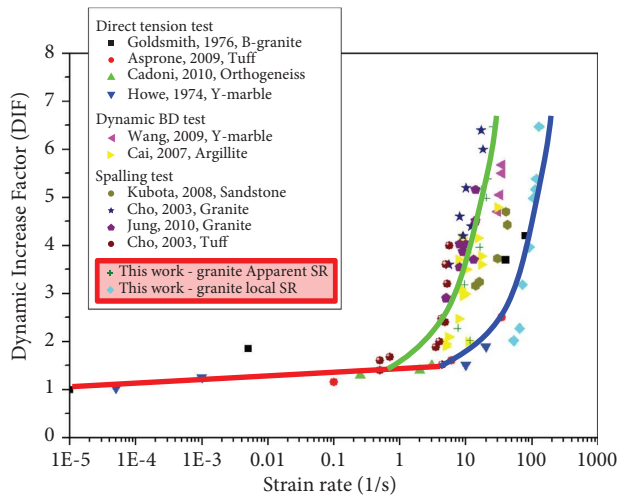

Figure 18: Comparison of the DIF from the dynamic tension tests [10, 11, 23–29].

apparent strain rates showed similar results to those of indirect tensile test methods performed in previous studies. On the other hand, the dynamic tensile strength values plotted at local strain rates indicate similar results to those estimated by the direct tensile test method. This suggests the importance of calculating the strain rate in the dynamic testing of rock materials and is considered a remarkable reference to the legislation of standard rock dynamic testing methods and the dynamic fracture behavior of the rock materials that have not been established to date.

5. Conclusion

In this study, the evaluation technique for the dynamic tensile strength using the spalling method was reviewed. In comparison with the results of the conventional dynamic BD test, the dynamic tensile strength estimated by the spalling test appeared good consistency with the results of the BD test. Therefore, it is believed that it can be used as a sufficient alternative test method for BD tests that cannot be performed under high strain rate conditions. Comparative reviews of dynamic tensile strength evaluation methods used in preceding research cases with respect to spalling tests were performed. As a result, Method A, which does not reflect the direct behavior of the specimen, is overvalued compared to the results of others. Comparisons between Method B and C that calculate tensile strength based on the measurement of the free surface behavior of the specimen revealed the problems in determining the failure plane of the specimen through macroscopic observations.

Spalling tests using different lengths of the specimens were conducted to identify problems with the conventional method of calculating the apparent strain rate. Compared to previous studies, the dynamic tensile strength values calculated through the apparent strain rate showed similarities with the results determined by the indirect tensile testing method, and the strength values calculated through the local strain rate were found to comply with the results evaluated by the direct tensile test method. This implies not only the

strength value of the rock materials, but also the influence of the method of calculating the strain rate on the evaluation of dynamic properties.

Data Availability

The experimental data used to support the findings of this study are included within the article.

Conflicts of Interest

The authors declare that they have no conflicts of interest.

Acknowledgments

This research was supported by the basic research project of the Korea Institute of Geoscience and Mineral Resources (KIGAM, GP2020-010) funded by the Ministry of Science and ICT, Korea.

References

[1] K. Xia and W. Yao, "Dynamic rock tests using split Hopkinson (Kolsky) bar system- a review," *Journal of Rock Mechanics and Geotechnical Engineering*, vol. 7, no. 1, pp. 27–59, 2015.

[2] Q. B. Zhang and J. Zhao, "A review of dynamic experimental techniques and mechanical behaviour of rock materials," *Rock Mechanics and Rock Engineering*, vol. 47, no. 4, pp. 1411–1478, 2014.

[3] F. Dai, *Dynamic Tensile, Flexural and Fracture Tests of Anisotropic Barre Granite*, Dissertation; University of Toronto, Toronto, Canada, Ph.D, 2010.

[4] R. Chen, K. Xia, F. Dai, F. Lu, and S. N. Luo, "Determination of dynamic fracture parameters using a semi-circular bend technique in split Hopkinson pressure bar testing," *Engineering Fracture Mechanics*, vol. 76, no. 9, pp. 1268–1276, 2009.

[5] Y. X. Zhou, K. Xia, X. B. Li et al., "Suggested methods for determining the dynamic strength parameters and Mode I fracture toughness of rock materials," *International Journal of Rock Mechanics and Mining Sciences*, vol. 49, pp. 105–112, 2012.

[6] F. Dai, S. Huang, K. Xia, and Z. Tan, "Some fundamental issues in dynamic compression and tension tests of rocks using split Hopkinson pressure bar," *Rock Mechanics and Rock Engineering*, vol. 43, no. 6, pp. 657–666, 2010.

[7] F. Dai, K. Xia, H. Zheng, and Y. Wang, "Determination of dynamic rock Mode-I fracture parameters using cracked chevron notched semi-circular bend specimen," *Engineering Fracture Mechanics*, vol. 78, no. 15, pp. 2633–2644, 2011.

[8] F. Dai and K. Xia, "Rate dependence of flexural tensile strength of laurentian granite," in *Proceedings Of the 3rd CANUS Rock MEchanics Symposium*, Toronto, Canada, May 2010.

[9] B. Erzar and P. Forquin, "An experimental method to determine the tensile strength of concrete at high rates of strain," *Experimental Mechanics*, vol. 50, no. 7, pp. 941–955, 2010.

[10] S. Kubota, Y. Ogata, Y. Wada, G. Simangunsong, H. Shimada, and K. Matsui, "Estimation of dynamic tensile strength of sandstone," *International Journal of Rock Mechanics and Mining Sciences*, vol. 45, no. 3, pp. 397–406, 2008.

[11] S. H. Cho, Y. Ogata, and K. Kaneko, "Strain-rate dependency of the dynamic tensile strength of rock," *International Journal of Rock Mechanics and Mining Sciences*, vol. 40, no. 5, pp. 763–777, 2003.

[12] K. Hino, "Velocity of rock fragmentation and shape of shock wave," *Journal of the Japan Explosives Society*, vol. 17, no. 4, pp. 236–241, 1956.

[13] J. R. Klepaczko and A. Brara, "An experimental method for dynamic tensile testing of concrete by spalling," *International Journal of Impact Engineering*, vol. 25, no. 4, pp. 387–409, 2001.

[14] H. Kolsky, "An investigation of the mechanical properties of materials at very high rates of loading," *Proceedings of the Physical Society Section B*, vol. 62, no. 11, pp. 676–700, 1949.

[15] S. Novikov, "Spall strength of materials under shock load," *Journal of Applied Mechanics and Technical Physics*, vol. 3, pp. 109–120, 1967.

[16] H. Schuler, C. Mayrhofer, and K. Thoma, "Spall experiments for the measurement of the tensile strength and fracture energy of concrete at high strain rates," *International Journal of Impact Engineering*, vol. 32, no. 10, pp. 1635–1650, 2006.

[17] F. Dai and K. Xia, "Loading rate dependence of tensile strength anisotropy of barre granite," *Pure and Applied Geophysics*, vol. 167, no. 11, pp. 1419–1432, 2010.

[18] Y. Nara and K. Kaneko, "Study of subcritical crack growth in andesite using the double torsion test," *International Journal of Rock Mechanics and Mining Sciences*, vol. 42, no. 4, pp. 521–530, 2005.

[19] Y. Nara, "Effect of anisotropy on the long-term strength of granite," *Rock Mechanics and Rock Engineering*, vol. 48, no. 3, pp. 959–969, 2015.

[20] F. Rodrigues, *Anisotropy of Granites. Modulus of Elasticity and Ultimate Strength Ellipsoids, Joint Systems, Slope Attitudes, and Their Correlationships*, 1st ISRM Congress, Lisbon, Portugal, 1966.

[21] Q. B. Zhang and J. Zhao, "Effect of loading rate on fracture toughness and failure micromechanisms in marble," *Engineering Fracture Mechanics*, vol. 102, pp. 288–309, 2013.

[22] F. Dai and K. W. Xia, "Laboratory measurements of the rate dependence of the fracture toughness anisotropy of Barre granite," *International Journal of Rock Mechanics and Mining Sciences*, vol. 60, pp. 57–65, 2013.

[23] W. Goldsmith, J. L. Sackman, and C. Ewerts, "Static and dynamic fracture strength of Barre granite," *International Journal of Rock Mechanics and Mining Sciences & Geomechanics*, vol. 13, no. 11, pp. 303–309, 1976.

[24] D. Asprone, E. Cadoni, A. Prota, and G. Manfredi, "Dynamic behavior of a mediterranean natural stone under tensile loading," *International Journal of Rock Mechanics and Mining Sciences*, vol. 46, no. 3, pp. 514–520, 2009.

[25] E. Cadoni, "Dynamic characterization of orthogneiss rock subjected to intermediate and high strain rates in tension," *Rock Mechanics and Rock Engineering*, vol. 43, pp. 667–676, 2010.

[26] S. Howe, W. Goldsmith, and J. L. Sackman, "Macroscopic static and dynamic mechanical properties of Yule marble," *Experimental Mechanics*, vol. 14, pp. 337–346, 1974.

[27] Q. Z. Wang, W. Li, and H. P. Xie, "Dynamic split tensile test of flattened Brazilian disc of rock with SHPB setup," *Mechanics of Materials*, vol. 41, no. 3, pp. 252–260, 2009.
[28] M. Cai, P. K. Kaiser, F. Suorineni, and K. Su, "A study on the dynamic behavior of the Meuse/Haute-Marne argillite," *Physics and Chemistry of the Earth, Parts A/B/C*, vol. 32, no. 8–14, pp. 907–916, 2007.
[29] W. Jung, "Effects of strain rate and water saturation on the tensile strength of rocks," *Tunnel & Underground Space*, vol. 20, no. 2, pp. 119–124, 2010.